

Preparation of $\text{La}_{0.6}\text{Ba}_{0.4}\text{Co}_{0.2}\text{Fe}_{0.8}\text{O}_3$ (LBCF) Nanoceramic Cathode Powders by Sol-Gel Process for Solid Oxide Fuel Cell (SOFC) Application

Yousef M. Al-Yousef, Mohammad Ghouse*

Energy Research Institute, King Abdulaziz City for Science and Technology (KACST), Riyadh, Saudi Arabia

E-mail: *msheikh@kacst.edu.sa, alyousef@kacst.edu.sa

Received January 29, 2011; revised March 14, 2011; accepted April 10, 2011

Abstract

The $\text{La}_{0.6}\text{Ba}_{0.4}\text{Co}_{0.2}\text{Fe}_{0.8}\text{O}_3$ (LBCF) nano ceramic powders were prepared by Sol-Gel process using nitrate based chemicals for SOFC applications since these powders are considered to be more promising cathode materials for SOFC. Citric acid was used as a chelant agent and ethylene glycol as a dispersant. The powders were calcined at $650^\circ\text{C}/6$ h, $900^\circ\text{C}/3$ h in air using Thermolyne 47,900 furnace. These powders were characterized by SEM/EDS, XRD and Porosimetry techniques. The SEM images indicate that the particle sizes of the LBCF powders are in the range of 50 - 200 nm. The LBCF perovskite phases are seen from the XRD patterns. From XRD Line broadening technique, the average particle size for the powders (as prepared and calcined at $650^\circ\text{C}/6$ h and $900^\circ\text{C}/3$ h) were found to be around 12.97 nm, 22.24 nm and 26 nm respectively. The surface area of the LBCF powders for the as prepared and calcined at 650°C were found to be 28.92 and $19.54\text{ m}^2/\text{g}$ respectively.

Keywords: XRD, SEM/EDS, $\text{La}_{0.6}\text{Ba}_{0.4}\text{Co}_{0.2}\text{Fe}_{0.8}\text{O}_3$ (LBCF), Porosimetry

1. Introduction

The Solid oxide fuel cells (SOFCs) are prominent candidates of power generators that convert chemical energy directly and with high efficiency, into electricity while causing little pollution. These power generating systems have attracted a considerable attention because of their environmental friendliness, and fuel flexibility [1,2]. The current status of the development of a cell unit is based on yttria-stabilized zirconia (YSZ) solid electrolyte and electrodes consisting of Sr-doped LaMnO_3 (Cathode) and Ni-YSZ cermet (Anode) [3,4]. Among the cathode materials reported (La, Sr) MnO_3 (LSM) based perovskite, due to their stability and high electrocatalytic activity for oxygen reduction at high temperatures, are the most extensively studied and investigated materials for O_2 reduction [5-9]. In spite of significant efforts by various researchers, fundamental questions on the mechanism and kinetics of the O_2 reduction reaction and on the electrode behavior of LSM materials under fuel-cell operation conditions still remain unsolved. Although LSM has shown promising performance for SOFC operating at temperature around 800°C , its performance decreases

rapidly as the operating temperature decreases [10]. Therefore, considerable research interest is currently directed towards cobalt containing perovskite oxides which tends to exhibit mixed-conduction characteristics and relatively higher ionic conductivities than LSM due to a greater concentration of oxygen vacancies [11-13]. Recently, several new compositions that show mixed ionic and electronic conductivity (MIEC) have been developed as promising SOFC cathodes [14-17]. Amongst these, the perovskite based compounds having the general formula $\text{La}_{1-x}\text{Sr}_x\text{M}_{1-y}\text{C}_y\text{O}_3$, where $0 \leq x \leq 0.5$ and $0 \leq y \leq 0.8$ (M is a transitional metal Mn or Fe) has found wide attention because of their superior MIEC behavior [15,16] as well as enhanced oxygen reduction reactions (ORR) kinetics [17-19].

Most recently $\text{Ba}_{0.5}\text{Sr}_{0.5}\text{Co}_{0.8}\text{Fe}_{0.2}\text{O}_3$ (BSCF) oxide has been found to exhibit excellent activity as a new cathode material as reported in [20]. Therefore replacing Sr with Ba in LSCF would reduce Cr deposition according to the proposed strategy [21,22] and to maintain high electrocatalytic activity for O_2 reduction reaction. Several researchers have reported different techniques [23-24] for preparing $\text{La}_{0.6}\text{Ba}_{0.4}\text{Co}_{0.2}\text{Fe}_{0.8}\text{O}_3$ (LBCF) materials for

SOFC cathode materials due to their attractive properties. **Table 1** shows the suitable materials for SOFC components [25].

The main design requirements for SOFC cathode materials [26] include: 1) High electronic conductivity; 2) Chemically compatible with neighboring cell components (electrolyte); 3) Stable in oxidizing environment; 4) Large triple phase boundary; 5) High ionic conductivity; 6) Thermal expansion coefficient similar to other SOFC materials; 7) Relative simple fabrication; 8) Relatively inexpensive materials.

In this paper, nanocrystalline LBCF powders for cathode material were prepared by the Sol-Gel process since it is a simple and more economical way of making nanopowders. The powders were characterized using SEM/EDS, XRD, porosimetry techniques.

2. Experimental Procedure

2.1. Preparation of LBCF Powders

The $\text{La}_{0.6}\text{Ba}_{0.4}\text{Co}_{0.2}\text{Fe}_{0.8}\text{O}_3$ (LBCF) nanoceramic powders were prepared by modified Sol-Gel Process [27-29] using $\text{La}(\text{NO}_3)_3 \cdot 6\text{H}_2\text{O}$ (BDH), $\text{Ba}(\text{NO}_3)_2$ (BDH), $\text{Co}(\text{NO}_3)_2 \cdot 9\text{H}_2\text{O}$ (Fluka), $\text{Fe}(\text{NO}_3)_3 \cdot 9\text{H}_2\text{O}$, citric acid (BDH) ethylene glycol (BDH), ammonia solution and distilled water. The precursor solution was prepared by mixing individual aqueous solutions of the above chemicals in a molar ratio of 0.6:0.4 and 0.2:0.8 respectively. To the mixed all nitrate solutions, required citric acid, ammonia solution and ethylene glycol were added. The citrate/nitrate (c/n) ratio used in the present experiments was 0.5. The solution was heated in a pyrex glass beaker on a hotplate using magnetic stirrer until a chocolate colored gel was formed. When heated further, the gel burns to a light fragile ash. The ash was calcined at $650^\circ\text{C}/6\text{ h}$, and $900^\circ\text{C}/3\text{ h}$ in air in a Barnstead Thermolyne 47900 Furnace (USA). **Figure 1** shows the flow Sheet for the preparation of $\text{La}_{0.6}\text{Ba}_{0.4}\text{Co}_{0.2}\text{Fe}_{0.8}\text{O}_3$ powder using the Sol-Gel process. **Table 2** shows cathode materials prepared by the Sol-Gel process.

2.2. SEM/EDS Characterization

Small amounts of the samples were spread on adhesive conductive aluminum tapes attached to sample holders, coated with thin films of gold and examined with a FEI Quanta 200 Scanning Electron Microscope. An attached OXFORD INCA250 Energy Dispersive Spectroscopy (EDS) unit was used to determine the area and spot elemental compositions. Images at higher magnification were collected with a FEI Quanta 3DF SEM. Imaging was performed in Secondary Electron (SEI) mode only using an accelerating voltage of 20 keV.

2.3. XRD Characterization

A part of the samples were analyzed with a PANnlytical X'Pert PRO XRD for phase characterization. The X-ray diffractometry with $\text{CuK}\alpha$ radiation at 35 KV and 20 mA was used for phase analysis with a diffraction angle 2θ range $10^\circ - 80^\circ$ and particle size determination from X-ray line broadening technique using the following Debye Scherrer Equation [30]:

$$t = 0.9\lambda/B \cos \emptyset$$

where t = average particle size in nm, λ = the wave length (0.15418 nm) of $\text{Cu K}\alpha$ radiation, B the width (in radian) of the XRD diffraction peak at half of its maximum intensity (FWHM), and \emptyset the Bragg diffraction angle of the line, and B is the line width at half peak intensity.

2.4. Porosimetry Characterization

2.4.1. Particle Size Distribution

Particle size distribution analysis was done using particle size analyzer Mastersizer 2000 manufactured by Malvern Instruments UK. This instrument works on the basis of laser diffraction and is equipped with Hydro 2000S liquid feeder with a capacity of 50 to 120 ml. The feeder has a built-in ultrasound probe with an inline pump and stirrer. The instrument is capable to measure particle size

Table 1. Suitable materials for SOFC components [25].

Component	Requirements	Preferred Materials	Possible Alternatives
Electrolyte	$\sigma_i > 0.05 \text{ S}\cdot\text{cm}^{-1}$	$\text{ZrO}_2\text{-Y}_2\text{O}_3$ (3 - 10 mol%)	$\text{ZrO}_2\text{-Sc}_2\text{O}_3$, $\text{CeO}_2\text{-Gd}_2\text{O}_3$, (Sm_2O_3)
Cathode	$>100 \text{ S}\cdot\text{cm}^{-1}$ (electronic/mixed)	$\text{La}_{1-x}\text{Sr}_x \text{MnO}_3$	$(\text{La}_{1-x}\text{Sr}_x)\text{Co}$, FeO_3
Anode	$>100 \text{ S}\cdot\text{cm}^{-1}$ (electronic/ mixed)	$\text{Ni/ZrO}_2\text{-Y}_2\text{O}_3$	$\text{Ru/ZrO}_2\text{-Y}_2\text{O}_3$ $\text{Ni/CeO}_2\text{-ZrO}_2\text{-M}_2\text{O}_3$ cermets
Interconnect	Inert material, high temperature stability	High temp. alloys $\text{La}_{1-x}(\text{Sr}, \text{Ca}, \text{Mg})_x\text{CrO}_3$	-
Manifold	Non-volatile, inert	Ceramics, metals	-
Seal	Non-volatile, inert	Glass, glass-ceramic, Metal/ceramic	-

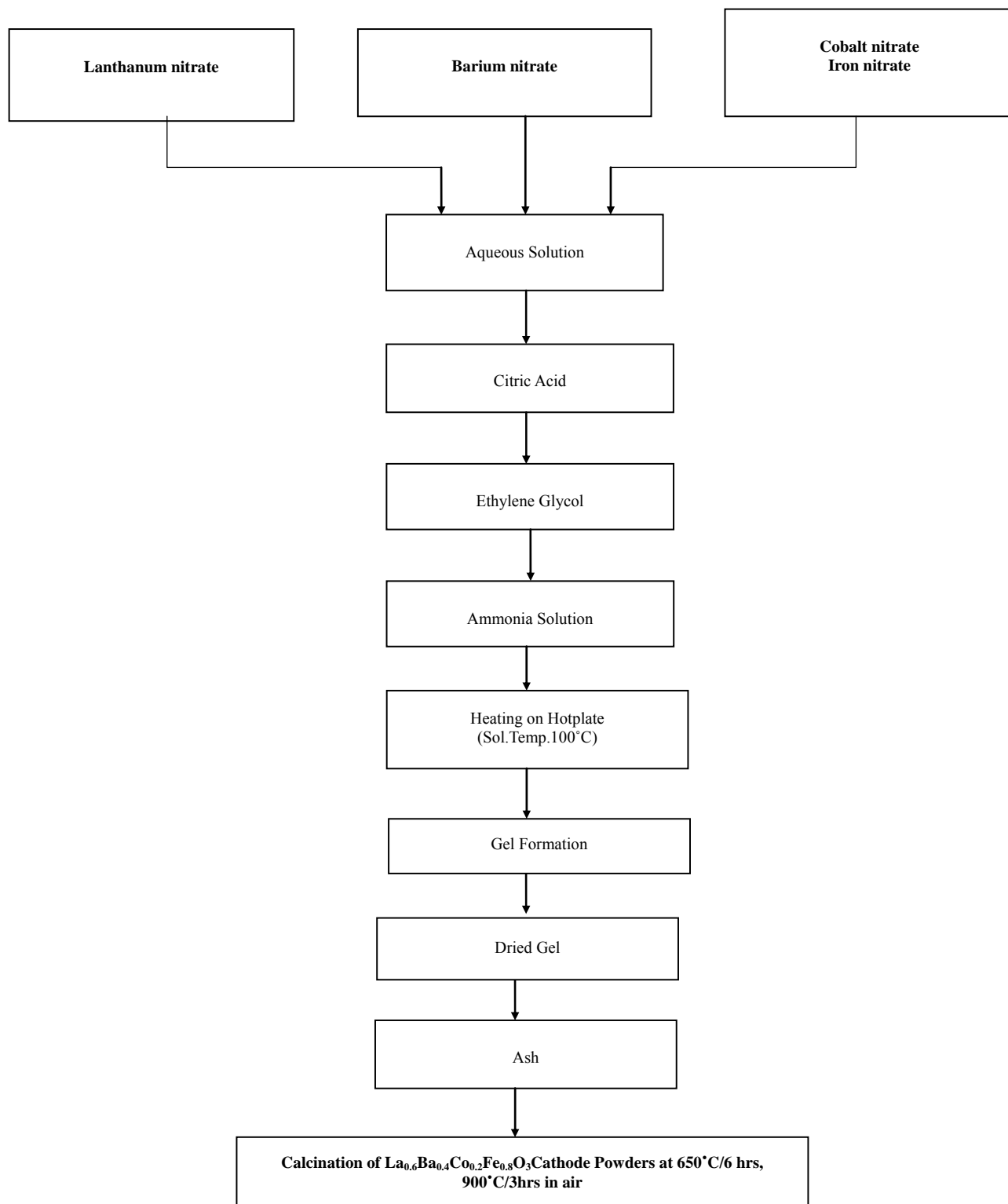


Figure 1. Flow sheet for the preparation of $\text{La}_{0.6}\text{Ba}_{0.4}\text{Co}_{0.2}\text{Fe}_{0.8}\text{O}_3$ nanoceramic Cathode Powders by Sol-Gel process [27-29].

distribution within a range of 0.02 to 2000 μm . Distilled water was used as a dispersant. The sample was added to the dispersant to an obscursion limit in the range of 5% -

20%. The calculation of particle size distribution was done using Mie theory. The samples were analyzed with and without ultrasound probe. The above instrument

Table 2. LBCF cathode powders prepared by Sol-Gel process.

Sample ID No	Cathode Powder
#72 a, b	$\text{La}_{0.6}\text{Ba}_{0.4}\text{Co}_{0.2}\text{Fe}_{0.8}\text{O}_3$
#76 a, b, c	$\text{La}_{0.6}\text{Ba}_{0.4}\text{Co}_{0.2}\text{Fe}_{0.8}\text{O}_3$

LBCF: a: as prepared; b: calcined at 650°C; and c: calcined at 900°C.

measures the particle size distribution on the basis of volume of sample particles.

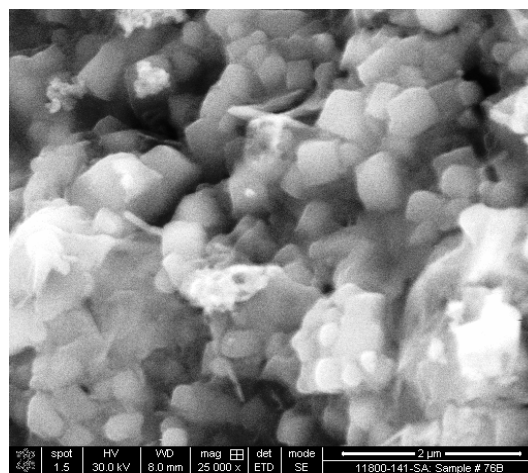
2.4.2. Surface Area, Pore Volume and Pore Size Measurement

The surface areas of samples were measured using an Autosorb-1C instrument manufactured by Quanta Chrome, USA. Samples were taken in the range of 0.1 - 0.2 g in a cell and were degassed at 300°C for 3 hrs to remove any absorbed material on the surface. Nitrogen gas was used as an adsorbent. The BJH cumulative adsorption method was used to calculate pore volume cc/gr and pore size in °A. The surface area (m^2/g) of the powder as prepared and calcined at 650°C were calculated.

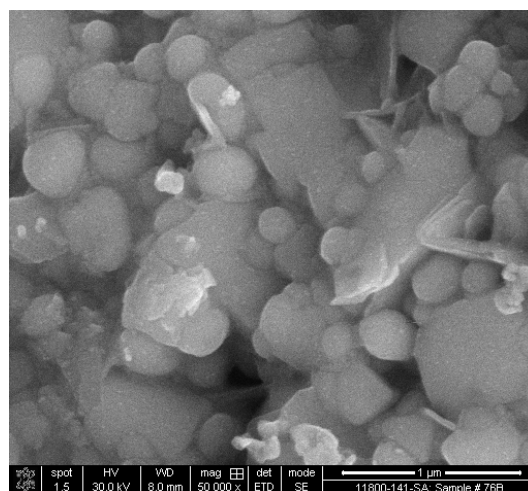
3. Results and Discussion

3.1. SEM/EDS Characterization

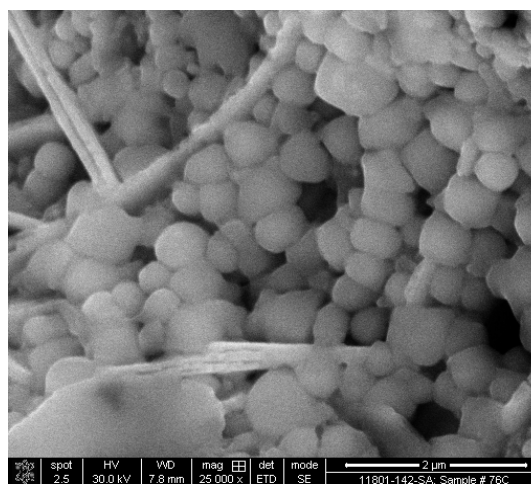
Figures 2(a)-2(c) show the nano-sized particles observed by Scanning electron microscopy from the $\text{La}_{0.6}\text{Ba}_{0.4}\text{Co}_{0.2}\text{Fe}_{0.8}\text{O}_3$ (LBCF) powder samples calcined under oxygen atmosphere at 650°C and 900°C which were prepared with the Sol-Gel process using metallic nitrates. It is seen in the SEM images that the particles are homogeneous with the presence of highly porous spherical particles with an approximate particle size between 50 - 200 nm. It is noted from the figures that the particle size of the calcined powders at 650°C and 900°C are larger than the as prepared powders as per expectation. It is also seen that by increasing the calcination temperature a well defined crystal structure develops (**Figure 2**). **Figures 3(a)** and **3(b)** show the EDS patterns of $\text{La}_{0.6}\text{Ba}_{0.4}\text{Co}_{0.2}\text{Fe}_{0.8}\text{O}_3$ powders. The figures show the presence of La, Ba, Co, Fe, C, O peaks. The residual C element from the citric acid that probably had not been combusted yet is shown in EDS in the as prepared powder. However, the C content has been reduced in the calcined powders at 900°C. By increasing the calcination temperature, the C is minimized further. The wt% of C, La, Ba, Co, Fe and O are presented in the tables through EDS analysis.



(a)

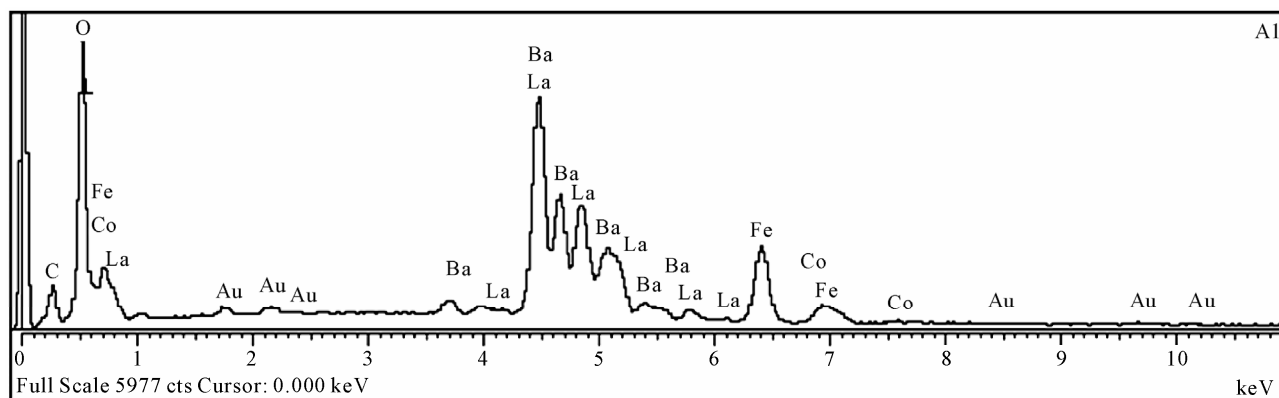


(b)



(c)

Figure 2. (a) SEM image of LBCF Cathode Powder calcined at 650°C (#76b); (b) SEM image of LBCF Cathode Powder calcined at 650°C (#76b); (c) SEM image of LBCF Cathode Powder calcined at 900°C (#76c).

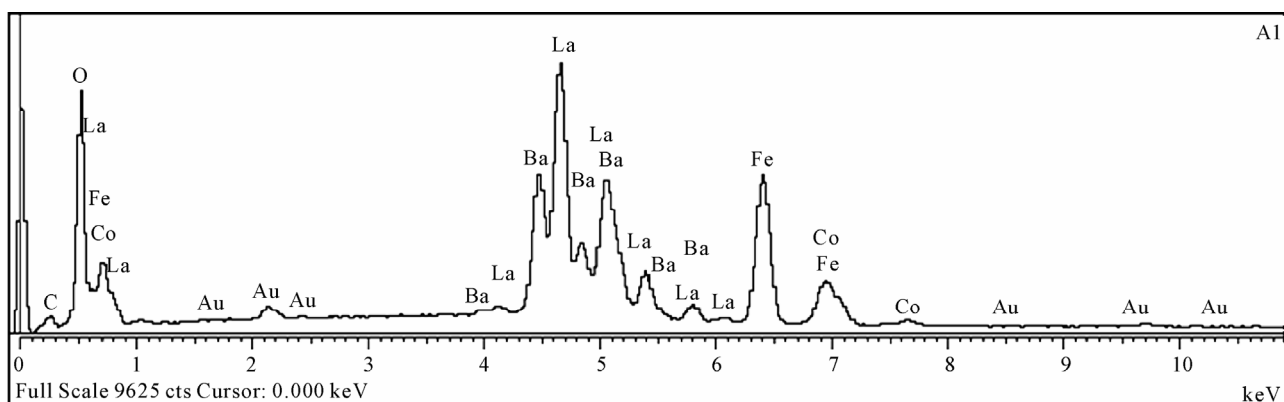


Processing option: all elements analysed (Normalised) #76b.

Spectrum	In stats.	C	O	Fe	Co	Ba	La	Total
A1	Yes	9.67	28.43	8.21	2.08	33.23	18.37	100.00
Mean		9.67	28.43	8.21	2.08	33.23	18.37	100.00
Std. deviation		0.00	0.00	0.00	0.00	0.00	0.00	
Max.		9.67	28.43	8.21	2.08	33.23	18.37	
Min.		9.67	28.43	8.21	2.08	33.23	18.37	

All results in weight%.

(a)



Processing option: all elements analysed (Normalised) #76c

Spectrum	In stats.	C	O	Fe	Co	Ba	La	Total
A1	Yes	3.55	12.90	7.71	2.89	49.39	23.56	100.00
Mean		3.55	12.90	7.71	2.89	49.39	23.56	100.00
Std. deviation		0.00	0.00	0.00	0.00	0.00	0.00	
Max.		3.55	12.90	7.71	2.89	49.39	23.56	
Min.		3.55	12.90	7.71	2.89	49.39	23.56	

All results in weight%.

(b)

Figure 3. (a) EDS of LBCF #76b (Calcined at 650°C); (b) EDS of LBCF #76d (Calcined at 900°C).

3.2. XRD Characterization

Figures 4(a)-(c) show the XRD patterns of the as prepared and calcined powders of $\text{La}_{0.6}\text{Ba}_{0.4}\text{Co}_{0.2}\text{Fe}_{0.8}\text{O}_3$ at 650°C and 900°C respectively. It is seen that there are expected phase present in the calcined powder. It is seen that the calcined powder has well crystalline perovskite phases of $\text{La}_{0.6}\text{Ba}_{0.4}\text{Co}_{0.2}\text{Fe}_{0.8}\text{O}_3$. Table 3 shows the particle sizes of LBCF powders calcined at 650°C and 900°C . It is seen that the particle size is increased by increasing the calcination temperatures as expected. The average grain size of as prepared and calcined (at 650°C and 900°C) powders are increased from 12 nm to 26 nm respectively. The X-ray line broadening technique can be used only for size determination of small crystallites (~ 100 nm). The values obtained here may not be true particle size. The crystallite size of the as prepared powders depends on the citrate to nitrate (c/n) ratio during combustion process [31]. The XRD results obtained here are in agreement with results reported elsewhere [23,24]. It is seen in Figure 4(c) that the crystallinity of the powders increased with sharp peaks by increasing the calcination temperature. However, it is observed only small

Table 3. XRD Data to determine the average particle size of the LBCF powders prepared by Sol-Gel.

S.no.	2θ	B FWHM	Particle size, t (nm)
76a	32.94	0.632	12.97
76b	32.32	0.368	22.24
76c	32.24	0.312	26.23

$$t = 0.9 \times \lambda / B \cos \theta, B = \text{FHHM in } ^\circ, B = [\text{FWHM}/180] \times [22/7] = \text{FWHM} \times 0.017460, \lambda (\text{Cu}) = 0.15418 \text{ nm.}$$

peaks which were attributed to the perovskite LaCoO_3 phase which could be eliminated by employing high purity (99.99%) metal nitrate chemicals. Compared with as prepared LBCF powder the XRD of calcined powder at 900°C is more crystallized perovskite LBCF sharp phase and could be used for cathode in SOFC application.

3.3. Porosimetry Characterization

Tables 4-7 show particle size (with and without ultrasound), average particle size, surface area, pore volume and pore size of the LBCF powders as prepared and cal-

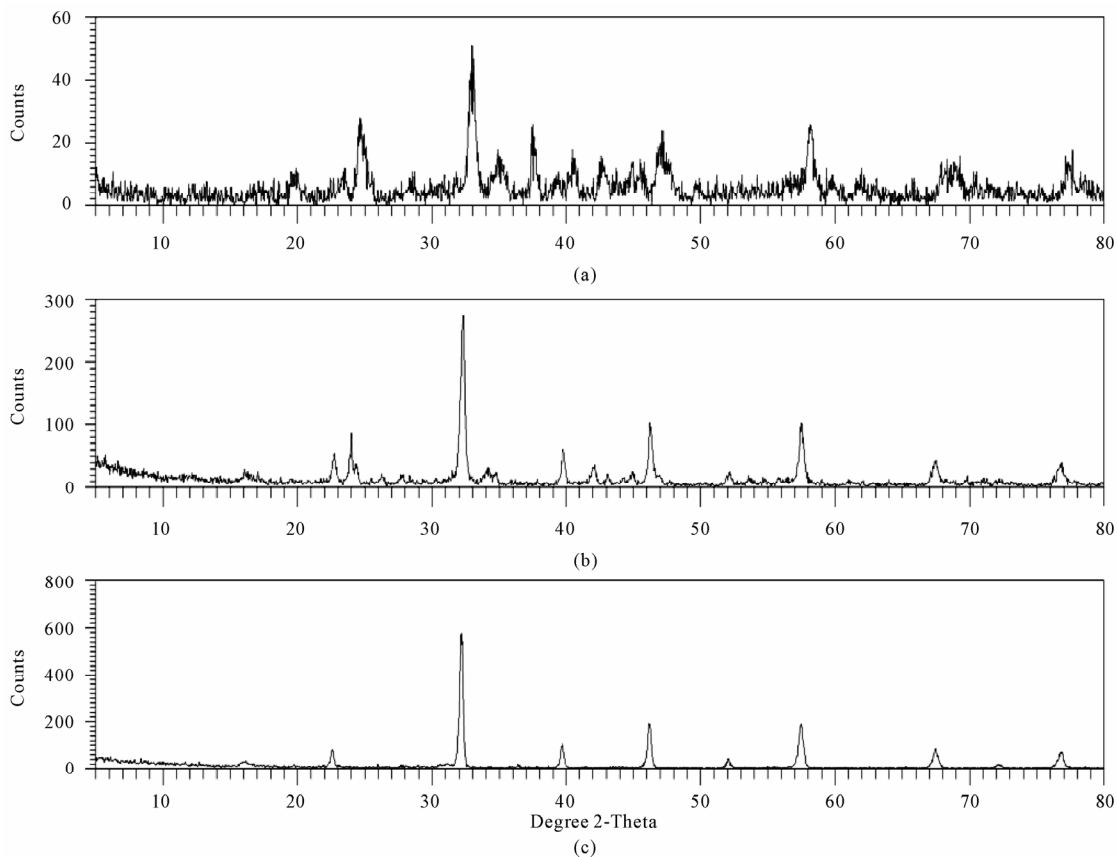


Figure 4. XRD pattern of $\text{La}_{0.6}\text{Ba}_{0.4}\text{Co}_{0.2}\text{Fe}_{0.8}\text{O}_3$ Cathode Powder # 76, (a) As prepared; (b) Calcined at 650°C ; (c) Calcined at 900°C .

Table 4. Particle size distribution of $\text{La}_{0.6}\text{Ba}_{0.4}\text{Co}_{0.2}\text{Fe}_{0.8}\text{O}_3$ powders (with ultrasound).

Sample ID Number	Volume Weighted Mean (μm)	
	With Ultrasound	Without Ultrasound
72 (a)	59.604	77.601
72 (b)	27.060	59.087

Table 5. Surface area data of $\text{La}_{0.6}\text{Ba}_{0.4}\text{Co}_{0.2}\text{Fe}_{0.8}\text{O}_3$ powders.

Sample ID Number	Surface Area (m^2/g)
72 (a)	28.92
72 (b)	19.54

Table 6. Pore volume data of $\text{La}_{0.6}\text{Ba}_{0.4}\text{Co}_{0.2}\text{Fe}_{0.8}\text{O}_3$ powders.

Sample ID Number	BJH Method Cumulative	Pore Volume (cc/g)
72 (a)	Adsorption	0.1168
	Desorption	0.1198
72 (b)	Adsorption	0.1495
	Desorption	0.1505

Table 7. Pore size data of $\text{La}_{0.6}\text{Ba}_{0.4}\text{Co}_{0.2}\text{Fe}_{0.8}\text{O}_3$ powders.

Sample ID Number	BJH Method	Pore Size ($^{\circ}\text{A}$)
72 (a)	Adsorption	65.75
	Desorption	38.33
72 (b)	Adsorption	22.42
	Desorption	17.52

calcined at 650°C) respectively. **Table 4** shows the average particle size of the powders before and after calcination. It is seen that without ultrasound the average particle size for the powders for both as prepared and calcined at 650°C is higher. **Table 5** shows that the surface area of the powders for as prepared and calcined at 650°C are $28.92 \text{ m}^2/\text{gr}$, $19.54 \text{ m}^2/\text{gr}$ respectively. It is seen that the calcined powders have lesser surface area as expected. The surface areas of the powders are similar to the surface areas of the commercially available nano powders [32]. From **Table 6** it is observed that there is marginal increase in the pore volume for calcined powder at 650°C . **Table 7** shows the pore size data of LBCF powders for adsorption (BJH method) has reduced for the calcined powders at 650°C . This may be again due to sintering at 650°C and subsequently shrinkage might have occurred. **Figures 5(a)-(d)** show the particle distribution of the

powders *i.e.* as prepared, calcined at 650°C respectively. It is seen from the **Table 4** and **Figures 5(a)-(d)** that the ultrasounds helped break the large agglomerates and narrowed the particle size distribution. Increasing the calcination temperature increased particle size (agglomerate size), but ultrasounds fragment the aggregates which indicates the agglomerates are soft which is observed due to the preparation with either Sol-Gel or any other soft chemical route like combustion synthesis. Actually with increase in temperature the agglomerate size should increase and surface area should decrease thereby. It is observed that even if there is a chance of soft agglomerates forming at higher calcination temperature, the effect is nullified by ultrasounds. However this needs further studies to correlate surface area results with particle size distribution and calcination temperatures.

4. Conclusions

The following conclusions are drawn from the present investigation:

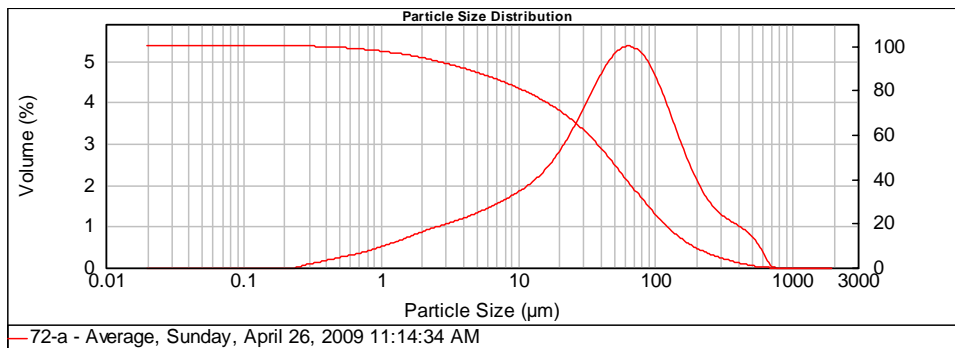
- The $\text{La}_{0.6}\text{Ba}_{0.4}\text{Co}_{0.2}\text{Fe}_{0.8}\text{O}_3$ (LBCF) nano ceramic powders for cathodes were successfully prepared by Sol-Gel process with c/n ratio of 0.5.
- SEM images indicate that the Particle size of LBCF powders are in the range of 50 - 200 nm.
- XRD patterns show the presence of the perovskite $\text{La}_{0.6}\text{Ba}_{0.4}\text{Co}_{0.2}\text{Fe}_{0.8}\text{O}_3$ phases.
- Porosimetry analysis shows the surface area reduced from $\sim 28.92 \text{ m}^2/\text{g}$ to $19.54 \text{ m}^2/\text{g}$ with calcining the powder at 650°C .

5. Acknowledgements

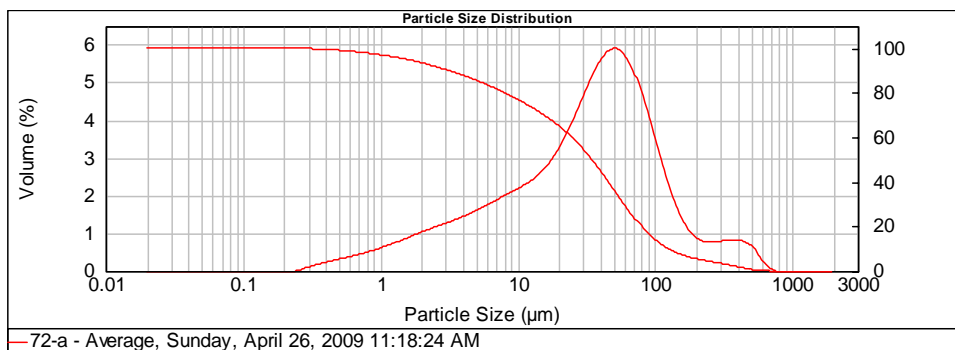
Authors thank Dr. Naif M. Al-Abbadi, former Director, Energy Research Institute, King Abdulaziz City for Science and Technology (KACST), Riyadh, Saudi Arabia for his encouragement and support during the course of this work.

Also, author's thanks are due to Mr. Mahmoud Al-Manea and Dr. Shahreer Ahmad, Technology Center (TC), Saudi Arabian Basic Industries Corporation (SABIC), Jubail, Saudi Arabia for providing SEM/EDS result of cathode powder samples. Author's thanks are due to Dr. Naseem Akhtar of Research Institute (RI), KFUPM, Dhahran, Saudi Arabia for providing Porosimetry analysis of the powders.

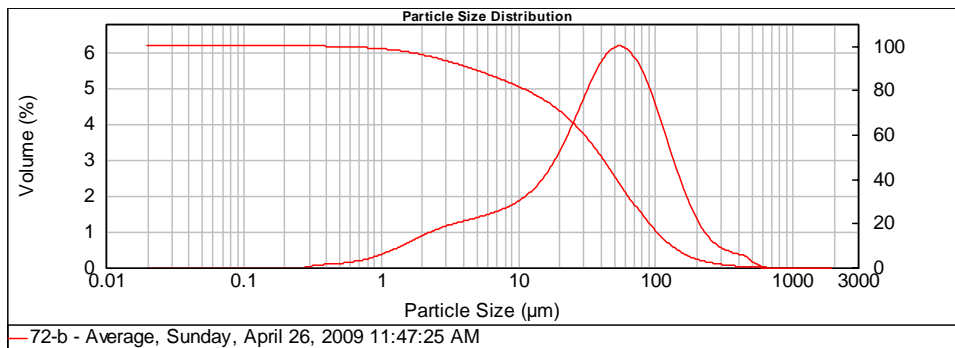
Also, author's thanks are due to Mr. Haitham Al-Gothami Technician, Atomic Energy Research Institute (AERI) KACST, Riyadh, Saudi Arabia for providing XRD analysis of Cathode powder samples. Author's thanks are due to Mr. Raed A. Al-Gumhan and Mr. Mansour Al-Saadon of Energy Research Institute, KACST for their assistance during the experiments.



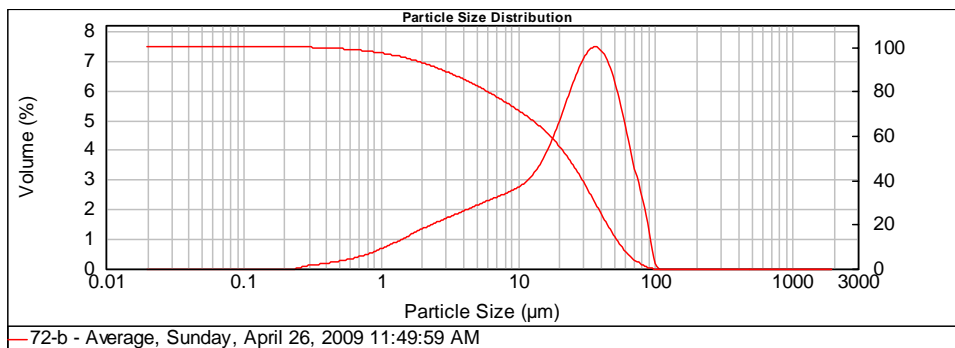
(a)



(b)



(c)



(d)

Figure 5. (a) Particle Size distribution of LBCF Cathode powders—without ultrasound; (b) Particle Size distribution of LBCF Cathode powders—with ultrasound; (c) Particle size distribution of LBCF Cathode powders—without ultrasound; (d) Particle size distribution of LBCF Cathode powders—with ultrasound 72a: as prepared, 72b: cycled at 650°C.

6. References

- [1] S. C. Singhal and K. Kendall, "High-Temperature Solid Oxide Fuel Cells: Fundamentals, Design and Applications," Elsevier Science, Oxford, 2003.
- [2] T.-L. Wen, D. Wang, M. Chen, H. Z. Zhang, H. Nie and W. Huang, "Material Research for Planar SOFC Stack," *Solid State Ionics*, Vol. 148, No. 3-4, 2002, pp. 513-519. [doi:10.1016/S0167-2738\(02\)00098-X](https://doi.org/10.1016/S0167-2738(02)00098-X)
- [3] N. Sakai, T. Kawada, H. Yokokawa, M. Dokia and T. Iwata, "Sinterability and Electrical Conductivity of Calcium-Doped Lanthanum Chromiyes," *Journal of Materials Science*, Vol. 25, No. 10, 1990, pp. 4531-4534. [doi:10.1007/BF00581119](https://doi.org/10.1007/BF00581119)
- [4] N. Sakai, T. Horita, H. Yokokawa, M. Dokiya and T. Kawada, "Oxygen Permeation Measurement of $\text{La}_{1-x}\text{CaCrO}_{3-x}$ by Using an Electrochemical Method," *Solid State Ionics*, 1996; Vol. 86-88, Part 2, pp. 1273-1278. [doi:10.1016/0167-2738\(96\)00300-1](https://doi.org/10.1016/0167-2738(96)00300-1)
- [5] T. Horita, K. Jamaji, M. Ishikawa, N. Sakai, H. Yokokawa and T. Kawada, "Active Sites Imaging for Oxygen Reduction at $\text{La}_{0.9}\text{Sr}_{0.1}\text{MnO}_{3-x}/\text{Yttria-Stabilized Zirconia}$ Interface by Secondary-Ion Mass Spectrometry," *Journal of the Electrochemical Society*, Vol. 145, No. 9, 1998, pp. 3196-3202.
- [6] J. Mizusaki, H. Tagawa, K. Naraya and T. Sasamoto, "Electronic Conductivity, Seebeck Coefficient, Defect and Electronic Structure of Nonstoichiometric $\text{La}_{1-x}\text{Sr}_x\text{MnO}_3$," *Solid State Ionics*, Vol. 132, No. 3-4, 2000, pp. 167-180. [doi:10.1016/S0167-2738\(00\)00662-7](https://doi.org/10.1016/S0167-2738(00)00662-7)
- [7] S. P. Jiang, J. P. Zhang, Y. Ramaprakash, D. Milosevic and K. Wilshier, "An Investigation of Shelf-Life of Strontium Doped LaMnO_3 Materials," *Journal of Materials Science*, Vol. 35, No. 11, 2000, pp. 735-741. [doi:10.1023/A:1004766212164](https://doi.org/10.1023/A:1004766212164)
- [8] S. P. Jiang, J. G. Love, J. P. Zhang, M. Hoang, Y. Ramaprakash and A. E. Hughes, "The Electrochemical Performance of LSM/Zirconia-Yttria Interface as a Function of a-Site Non-stoichiometry and Cathodic Current Treatment," *Solid State Ionics*, Vol. 121, No. 1-4, 1999, pp. 1-10. [doi:10.1016/S0167-2738\(98\)00295-1](https://doi.org/10.1016/S0167-2738(98)00295-1)
- [9] P. Decorse, G. Caboche and L.-C. Dufour, "A Comparative Study of the Surface and Bulk Properties of Lanthanum-Strontium-Manganese Oxides $\text{La}_{1-x}\text{Sr}_x\text{MnO}_{3\pm\delta}$ as a Function of Sr-Content, Oxygen Potential and Temperature," *Solid State Ionics*, Vol. 117, No. 1-2, 1999, pp. 161-169. [doi:10.1016/S0167-2738\(98\)00260-4](https://doi.org/10.1016/S0167-2738(98)00260-4)
- [10] Z. Tang, Y. Xie, H. Hawthorne and D. Ghosh, "Sol-Gel Processing of $\text{Sr}_{0.5}\text{Sm}_{0.5}\text{CoO}_3$ Film," *Journal of Power Sources*, Vol. 157, No. 1, 2006, pp. 385-388. [doi:10.1016/j.jpowsour.2005.07.041](https://doi.org/10.1016/j.jpowsour.2005.07.041)
- [11] B. C. H. Steele, "Appraisal of $\text{LCe}_{1-y}\text{Gd}_y\text{O}_{2-y/2}$ Electrolytes for IT-SOFC Operation at 500°C ," *Solid State Ionics*, Vol. 129, No. 1-4, 2000, pp. 95-110. [doi:10.1016/S0167-2738\(99\)00319-7](https://doi.org/10.1016/S0167-2738(99)00319-7)
- [12] E. B. Mitberg, M. V. Patrakeev, I. A. Leonidov, V. L. Kozhevnikov and K. R. Poeppelmeier, "High-Temperature Electrical Conductivity and Thermopower in Nonstoichiometric $\text{La}_{1-x}\text{Sr}_x\text{CoO}_{3-\delta}$ ($x = 0.6$)," *Solid State Ionics*, Vol. 127, No. 3-4, 2000, pp. 325-330. [doi:10.1016/S0167-2738\(00\)00670-6](https://doi.org/10.1016/S0167-2738(00)00670-6)
- [13] C.-F. Kao and C.-L. Zheng, "Electrochemical Behaviour of Oxygen at Nickel Nest Cathodic Material with Catalyst $\text{La}_{1-x}\text{Sr}_x\text{CoO}_3$," *Solid State Ionics*, Vol. 120, No. 1-4, 1999, pp. 163-171. [doi:10.1016/S0167-2738\(98\)00561-X](https://doi.org/10.1016/S0167-2738(98)00561-X)
- [14] S. P. Simner, J. F. Bonnett, N. L. Canfield, K. D. Meinhardt, V. L. Sprenkle and J. W. Stevenson, "Optimized Lanthanum Ferrite-Based Cathodes for Anode-Supported SOFCs," *Electrochemical and Solid-State Letters*, Vol. 5, No. 7, 2002, pp. 173-175.
- [15] A. Mai, V. A. C. Haanappel, S. Uhlenbruck, F. Tietz and D. Stover, "Ferrite-Based Perovskites as Cathode Materials for Anode-Supported Solid Oxide Fuel Cells: Part I. Variation of Composition," *Solid State Ionics*, Vol. 176, No. 15-16, 2005, pp. 341-350. [doi:10.1016/j.ssi.2005.03.009](https://doi.org/10.1016/j.ssi.2005.03.009)
- [16] Y. Teraoka, H. M. Zhang, K. Okamoto and N. Yamazoe, "Mixed Ionic -Electronic Conductivity of $\text{La}_{1-x}\text{Sr}_x\text{Co}_{1-y}\text{Fe}_y\text{O}_{3-x}$ Perovskite-Type Oxide," *Materials Research Bulletin*, Vol. 23, No. 1, 1988, pp. 51-58. [doi:10.1016/0025-5408\(88\)90224-3](https://doi.org/10.1016/0025-5408(88)90224-3)
- [17] J. A. Kilner, R. A. De Souza and I. C. Fullarton, "Surface Exchange of Oxygen in Mixed Conducting Perovskite Oxide," *Solid State Ionics*, Vol. 86-88, Part 2, 1996, pp. 703-709. [doi:10.1016/0167-2738\(96\)00153-1](https://doi.org/10.1016/0167-2738(96)00153-1)
- [18] S. Tanasescu, N. D. Totir and I. Marchidan, "Thermodynamic Properties of Some Perovskite Type Oxide Used as SOFC Cathode Materials," *Solid State Ionics*, Vol. 119, No. 1-4, 1999, pp. 311-315. [doi:10.1016/S0167-2738\(98\)00520-7](https://doi.org/10.1016/S0167-2738(98)00520-7)
- [19] J. Holc, D. Kušcer, M. Hrovat, S. Bernik and D. Kolar, "Electrical and Microstructural Characterization of $(\text{La}_{0.8}\text{Sr}_{0.2})(\text{Fe}_{1-x}\text{Al}_x)\text{O}_3$ and $(\text{La}_{0.8}\text{Sr}_{0.2})(\text{Mn}_{1-x}\text{Al}_x)\text{O}_3$ as Possible SOFC Cathode Materials," *Solid State Ionics*, Vol. 95, No. 3-4, 1997, pp. 259-268. [doi:10.1016/S0167-2738\(96\)00595-4](https://doi.org/10.1016/S0167-2738(96)00595-4)
- [20] Z. P. Shao and S. M. Haile, "A High-Performance Cathode for the Next Generation of Solid Oxide Fuel Cells," *Nature*, Vol. 431, 2004, pp. 170-173. [doi:10.1038/nature02863](https://doi.org/10.1038/nature02863)
- [21] Y. D. Zhen, A. I. Y. Tok, S. P. Jiang and F. Boey, " $\text{La}(\text{Ni},\text{Fe})\text{O}_3$ as a Cathode Material with High Tolerance to Chromium Poisoning for Solid Oxide Fuel Cells," *Journal of Power Sources*, Vol. 170, No. 1, 2007, pp. 61-66. [doi:10.1016/j.jpowsour.2007.03.079](https://doi.org/10.1016/j.jpowsour.2007.03.079)
- [22] Y. D. Zhen, S. P. Jiang and A. I. Y. Tok, "Strategy of the Development of Cr-Tolerant Cathodes of Solid Oxide Fuel Cells," *ECS Transactions*, Vol. 7, No. 1, 2007, pp. 263-269. [doi:10.1149/1.2729100](https://doi.org/10.1149/1.2729100)
- [23] S. Lee, Y. Lim, E. A. Lee, H. J. Hwang and J.-W. Moon, " $\text{Ba}_{0.5}\text{Sr}_{0.5}\text{Co}_{0.8}\text{Fe}_{0.2}\text{O}_{3-\delta}$ (BSCF) and $\text{La}_{0.6}\text{Ba}_{0.4}\text{Co}_{0.2}\text{Fe}_{0.8}\text{O}_{3-\delta}$ (LBCF) Cathodes Prepared by Combined Citrate-EDTA Method for IT-SOFCs," *Journal of Power Sources*, Vol. 157, No. 2, 2006, pp. 848-854. [doi:10.1016/j.jpowsour.2005.12.028](https://doi.org/10.1016/j.jpowsour.2005.12.028)
- [24] Y. Zhen and S. P. Jiang, "Characterization and Perform-

- ance of (La,Ba)(Co,Fe)O₃ Cathode for Solid Oxide Fuel Cells with Iron-Chromium Metallic Interconnect,” *Journal of Power Sources*, Vol. 180, No. 2, 2008, pp. 695-703. [doi:10.1016/j.jpowsour.2008.02.093](https://doi.org/10.1016/j.jpowsour.2008.02.093)
- [25] [http://azom.com.details.asp?ArticleID=157](http://azom.com/details.asp?ArticleID=157)
- [26] K. C. Wincewicz and J. S. Cooper, “Taxonomies of SOFC Material and Manufacturing Alternatives,” *Journal of Power Sources*, Vol. 140, No. 2, 2005, pp. 280-296.
- [27] M. Ghouse, A. Al-Musa, Y. Al-Yousef and M. F. Al-Otaibi, “Synthesis of Mg Doped LaCrO₃ Nano Powders by Sol-Gel Process for Solid Oxide Fuel Cell Application,” *Journal of New Materials for Electrochemical Systems*, Vol. 13, No. 2, 2010, pp. 99-106.
- [28] M. Ghouse, Y. Al-Yousef, A. Al-Musa and M. F. Al-Otaibi, “Preparation of La_{0.6}Sr_{0.4}Co_{0.2}Fe_{0.8}O₃ Nanoceramic Cathode Powders for Solid Oxide Fuel Cell (SOFC) Application,” *International Journal of Hydrogen Energy*, Vol. 35, No. 17, 2010, pp. 9411-9419. [doi:10.1016/j.ijhydene.2010.04.144](https://doi.org/10.1016/j.ijhydene.2010.04.144)
- [29] M. Ghouse, Y. Al-Yousef, A. Al-Musa and M. F. Al-Otaibi, “Preparation of La_{0.7}Ca_{0.3}CrO₃ Nanoceramic Powders for Solid Oxide Fuel Cell (SOFC) Application,” *World Journal of Engineering*, Vol. 6, No. 1, 2009, pp. 149-155.
- [30] B. D. Cullity, “Elements of X-Ray Diffraction,” 2nd Edition, Addison-Wesley Publication Co., Reading, 1978, p. 102.
- [31] R. D. Purohit, S. Saha and A. K. Tyagi “Nanocrystalline thoria Powders via Glycine-Nitrate Combustion,” *Journal of Nuclear Materials*, Vol. 288, No. 1, 2001, pp. 7-10. [doi:10.1016/S0022-3115\(00\)00717-0](https://doi.org/10.1016/S0022-3115(00)00717-0)
- [32] <http://www.advancedmaterials.us/S572726Sr.htm>